$\overline{1}$01 contact twins in gypsum experimentally obtained from calcium carbonate enriched solutions: mineralogical implications for natural gypsum deposits

Andrea Cotellucci,[a]* Fermín Otálora,[b] Àngels Canals,[c] Joaquin Criado-Reyes,[b] Luca Pellegrino,[a] Marco Bruno,[a] Dino Aquilano,[a] Juan Manuel Garcia-Ruiz,[b] Francesco Dela Pierre[a] and Linda Pastero[a]

[a]Dipartimento di Scienze della Terra, Università degli Studi di Torino, Via Valperga Caluso 35, Torino 10125, Italy, [b]Instituto Andaluz de Ciencias de la Tierra, CSIC-UGR, Avda De las Palmeras 4, Granada, Armilla 18100, Spain, and [c]Departament de Mineralogía, Petrología i Geología Aplicada, Facultat de Ciencies de la Terra, Universidad de Barcelona, Martí i Franqués 1, Barcelona 08028, Spain. *Correspondence e-mail: andrea.cotellucci@unito.it

Gypsum twins are frequently observed in nature, triggered by a wide array of impurities that are present in their depositional environments and that may exert a critical role in the selection of different twin laws. Identifying the impurities able to promote the selection of specific twin laws has relevance for geological studies aimed at interpreting the gypsum depositional environments in ancient and modern deposits. Here, the effect of calcium carbonate ($CaCO_3$) on gypsum ($CaSO_4 \cdot 2H_2O$) growth morphology has been investigated by performing temperature-controlled laboratory experiments with and without the addition of carbonate ions. The precipitation of twinned gypsum crystals has been achieved experimentally ($\overline{1}$01 contact twin law) by adding carbonate to the solution, and the involvement of rapidcreekite ($Ca_2SO_4CO_3 \cdot 4H_2O$) in selecting the $\overline{1}$01 gypsum contact twin law was supported, suggesting an epitaxial mechanism. Moreover, the occurrence of $\overline{1}$01 gypsum contact twins in nature has been suggested by comparing the natural gypsum twin morphologies observed in evaporitic environments with those obtained in experiments. Finally, both orientations of the primary fluid inclusions (of the negative crystal shape) with respect to the twin plane and the main elongation of sub-crystals that form the twin are proposed as a fast and useful method (especially in geological samples) to distinguish between the 100 and $\overline{1}$01 twin laws. The results of this study provide new insights into the mineralogical implications of twinned gypsum crystals and their potential as a tool to better understand natural gypsum deposits.

1. Introduction

Gypsum (calcium sulfate dihydrate, $CaSO_4 \cdot 2H_2O$) is the most abundant natural sulfate mineral on Earth's surface (Aquilano *et al.*, 2016) and is mostly found in evaporitic environments (*e.g.* Warren, 1982; Manzi *et al.*, 2009; Ortí, 2011; Lugli *et al.*, 2010; Van Driessche *et al.*, 2019; Costanzo *et al.*, 2019; Otálora *et al.*, 2020). Remarkably, the history of Earth, from the Neoproterozoic to the Phanerozoic, is punctuated by dramatic episodes of evaporitic deposition which resulted in the accumulation of thick gypsum or anhydrite-bearing sedimentary successions (*e.g.* Warren, 2010). Furthermore, gypsum deposits were also detected on Mars (Gendrin *et al.*, 2005; Langevin *et al.*, 2005), and a swallowtail gypsum habit, commonly referred to gypsum twins (Cody & Cody, 1989b), was recently observed by the NASA Curiosity Mars rover (Edgar *et al.*, 2018).

$\overline{1}$01 contact twin — 105°
[001] [101] — 40 μm
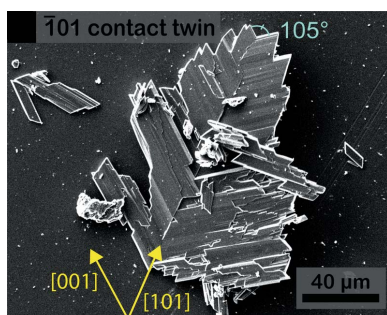
Depending on the depositional environment, gypsum exhibits different habits. In soils (Jafarzadeh & Burnham, 1992), desert regions (Shahid & Abdelfattah, 2009) and salt lakes (Warren, 1982; Mees *et al.*, 2012), tabular, prismatic, acicular, lenticular and twinned crystals are observed. In marine evaporites, mostly twinned and tabular gypsum crystals are found (Ortí, 2011), whereas the most spectacular habits are related to the anhydrite–gypsum thermally driven transformation by a self-feeding mechanism in low supersaturated solutions. This latter condition induces the precipitation of the prismatic metre-sized single crystals and twins of the Naica Mine (Mexico) (García-Ruiz *et al.*, 2007; Otálora & García-Ruiz, 2014) and in the Geode of Pulpì (Almería, Spain) (Canals *et al.*, 2019).

Many crystal-growth experiments have been performed to establish which conditions favor particular gypsum habits. Acicular gypsum single crystals were observed (i) in a gel medium (Rinaudo *et al.*, 1985), (ii) from the hydration of bassanite (Craker & Schiller, 1962) and (iii) by evaporation of Ca^{2+}–SO_4^{2-} rich water solutions at 35°C (Montagnino *et al.*, 2011), to name a few. Reiss *et al.* (2019) observed that saline waters with Na^+, K^+, Mg^{2+}, Sr^{2+}, Cl^- and Br^- ions in solution reduce the [001] elongation of gypsum single crystals, which switch from the acicular to the tabular habit, whereas organic molecules from the decomposition of green plants promote the lenticular habit (Cody, 1979). Regarding gypsum twins, both 100 and $\overline{1}01$ penetration twin laws of gypsum are common in pure aqueous solutions (Kern & Rehn, 1960), whereas α-amylase triggers the precipitation of a peculiar gypsum twin habit similar to those present in the Eocene deposits of the Paris Basin (Cody & Cody, 1989*a*; Van Driessche *et al.*, 2019).

An epitaxial relationship between the {010} pinacoid of gypsum and the {10.4} rhombohedron of calcite (Ruiz-Agudo *et al.*, 2016; Aquilano *et al.*, 2022) has been demonstrated. Therefore, the effect of carbonate anions – ubiquitous in evaporitic environments – on the habit of gypsum crystals deserves further investigation. Consequently, the main objective of this work is to explore the effect of calcium carbonate (Ca-carbonate, hereinafter) on the gypsum habit by performing temperature-controlled laboratory experiments from aqueous solutions with Ca-carbonate added and not added. Our results indicate that an aqueous solution saturated in Ca-carbonate promotes the precipitation of twinned gypsum following the $\overline{1}01$ contact twin law. To our knowledge, this is the first evidence of the effect of Ca-carbonate as a specific impurity in promoting the formation of the $\overline{1}01$ contact twin law.

Rapidcreekite was detected as a precursor in gypsum precipitation when carbonate species are dissolved in solution (Bots, 2011). The structural affinities between these two minerals suggest that rapidcreekite could act as a precursor of gypsum via an epitaxial mechanism, promoting the formation of the $\overline{1}01$ gypsum contact twin law.

Finally, we propose that the orientations of the negative crystal shape of primary fluid inclusions (FIs) with respect to the twin plane and the main direction of elongation of the sub-crystals that make up the twin are a useful tool to distinguish between 100 and $\overline{1}01$ twins, which can be relevant for the interpretation of ancient gypsum deposits.

2. Materials and methods

$CaSO_4 \cdot 2H_2O$ reagent plus ($\geq$99% Sigma–Aldrich), $CaCO_3$ ACS reagent ($\geq$99% powder, Sigma–Aldrich) and ultrapure water (18 MΩ, obtained using an Elga Purelab Flex3 water purification system) were used to prepare (i) $CaSO_4 \cdot 2H_2O$ saturated solution (G1) and (ii) $CaSO_4 \cdot 2H_2O$–$CaCO_3$ saturated solution (G2). Both G1 and G2 were saturated at 40°C. A cryo-compact Julabo circulator (CF31 series) was used to keep the solution at 40°C. Solubility values of $CaSO_4 \cdot 2H_2O$ at temperatures of 40 and 4°C were calculated using *PHREEQC* (version 3.7.3; Parkhurst & Appelo, 2013) and the default phreeqc database.

G1 was prepared by adding solid $CaSO_4 \cdot 2H_2O$ in amounts exceeding the saturation in pure water at 40°C (*i.e.* 2.66 g l^{-1}). G2 was prepared by adding $CaSO_4 \cdot 2H_2O$ in amounts exceeding its saturation in pure water at 40°C to a solution already saturated with Ca-carbonate. Under these conditions, the surplus of $CaCO_3$ and $CaSO_4 \cdot 2H_2O$ was stirred continuously in the flask for 15 days to ensure that saturation had been reached.

The pHs of G1 and G2 were 5.6 and 7.8, respectively. The pH of G2 is higher than that of G1 due to the basic hydrolysis of carbonate ions. pH measurements were carried out with a HANNA HI211 pH-meter.

Before the crystallization experiments, G1 and G2 were vacuum filtered in a beaker pre-heated to 40°C – to avoid rapid crystal precipitation – using a cellulose filter with a 0.45 μm pore size to remove any pre-existent $CaCO_3$ and $CaSO_4 \cdot 2H_2O$ particles.

Volumes of 100 ml of G1 and G2 were placed in a refrigerator set at 4°C for 30 days in closed flasks to avoid evaporation. Gypsum precipitation was achieved through different $CaSO_4 \cdot 2H_2O$–$CaCO_3$ solubilities as a function of temperature. Lowering the temperature from 40 to 4°C caused a decrease in gypsum solubility – from 2.66 to 2.29 g l^{-1} – and an increase in $CaCO_3$ solubility (Plummer & Busenberg, 1982; Coto *et al.*, 2012). Thus, Ca-carbonate minerals do not precipitate while both nucleation and growth of gypsum crystals occur.

Crystals were washed with ultrapure water, dried overnight at room temperature, and then analyzed by optical (Olympus BX4 with JENOPTIK ProgResC5 digital camera) and electron microscopes (JEOL JSM-IT300LV), equipped with a secondary, backscattered electron and energy-dispersive X-ray spectrometer.

Historically, gypsum was indexed in a variety of near-equivalent ways (*e.g.* Cole & Lancucki, 1974; Pedersen & Semmingsen, 1982; Comodi *et al.*, 2008). A comparison of these indexing possibilities is presented by Aquilano *et al.* (2016). Here, we adopted the monoclinic *C*2/*c* space group where a_0 = 5.63 Å, b_0 = 15.15 Å, c_0 = 6.23 Å, $\alpha = \gamma = 90°$, $\beta = 113.50°$ (De Jong & Bouman, 1939). Our choice was based on

two practical reasons: (i) this frame uses the smallest lattice vectors, and (ii) the [001] *z* axis coincides with the morphological elongation of the crystals growing from pure aqueous solution and the majority of natural crystals.

Figure 1
Geometry of contact and penetration twins, viewed along the [010] direction of gypsum. Modified from the work of Rubbo *et al.* (2012*a*,*b*) with permission from the American Chemical Society. Twin laws: 100, $\overline{1}01$, 001, $20\overline{1}$ and 101. For each twin law, the re-entrant angle value (θ) and the optical extinction angle value (Δ) have been reported. The extinction angles (Δ) were measured having adopted the structure defined by De Jong & Bouman (1939). The steps followed to measure the extinction angles are reported in Figs. S2 and S3 of the supporting information. Subscripts 'P' (parent) and 'T' (twinned) identify the two individuals that make up the twin.

3. Results and discussions

3.1. Gypsum twin growth morphologies

Five different twin laws are possible for the gypsum structure (Follner *et al.*, 2002), and each twin law is described by a contact and penetration twin (Rubbo *et al.*, 2012*a*,*b*). Thus, at least ten different twin habits are related to gypsum (Fig. 1).

Geometrically, each twin law is characterized by a specific re-entrant angle (Fig. 1). By measuring its value, we can identify the twin law. However, the 100 and $\overline{1}01$ twin laws have the same re-entrant angle (*i.e.* 105.02°). Thus, goniometry cannot distinguish these twins, and the formal way to correctly identify the 100 and $\overline{1}01$ twin laws requires the measurement of the extinction angle (Δ) formed between the two individuals, by means of optical microscopy with crossed polarizers. This angle is 14 and 26° for the 100 and $\overline{1}01$ twin laws, respectively. In addition, 100 and $\overline{1}01$ penetration twins are recognized by their different habits: 100 penetration twins are more acicular than $\overline{1}01$ penetration twins (Fig. 1).

Finally, a re-entrant angle and an arrowhead at opposite sides indicate a contact twin (Rubbo *et al.*, 2012*a*), while two re-entrant angles observed at the opposite twin sides identify a penetration twin (Rubbo *et al.*, 2012*a*,*b*).

From the G1 solution (saturated in CaSO$_4$·2H$_2$O) we obtained the precipitation of (i) acicular single crystals elongated along [001] [Fig. 2(*a*)], (ii) 100 penetration twins with the two re-entrant angles developing along [001] and [00$\overline{1}$] [Fig. 2(*b*)], and (iii) $\overline{1}01$ penetration twins with the two re-entrant angles developing along [101] and [$\overline{1}0\overline{1}$] [Fig. 2(*c*)].

From the G2 solution (saturated in CaSO$_4$·2H$_2$O and CaCO$_3$) we precipitated acicular crystals, 100 penetration twins and $\overline{1}01$ penetration twins (described above for the G1 solution), as well as a new twin morphology. Fig. 3(*a*) shows a twin characterized by a re-entrant angle of 105° and an optical extinction angle of 26° measured by means of optical microscopy (see Fig. S1 of the supporting information for the optical microscopy image). Moreover, a re-entrant angle at one side and an arrowhead at the opposite twin side are clearly observable. These features identify the $\overline{1}01$ contact twin law.

Both 100 and $\overline{1}01$ twin laws show the same re-entrant angle value. However, the sub-crystals composing 100 contact twins grow parallel to the twin plane (Otálora & García-Ruiz, 2014),
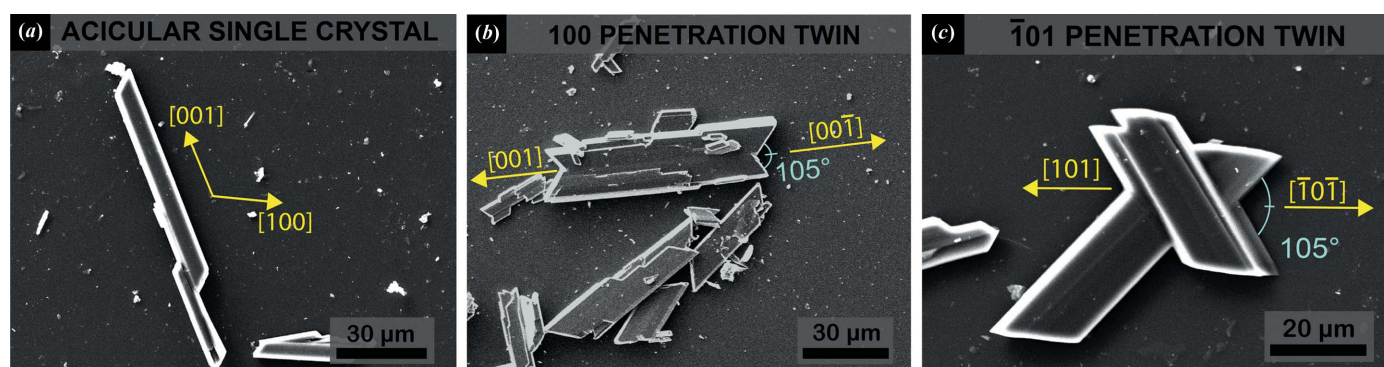

Figure 2
Gypsum crystals precipitated from G1 solution. (*a*) Acicular gypsum single crystals. (*b*) 100 penetration twin. (*c*) $\overline{1}01$ penetration twin.

whereas in $\overline{1}01$ contact twins the main elongation of sub-crystals is oriented obliquely with respect to the twin plane (Fig. 3). Therefore, we propose that the main elongation of the sub-crystals forming the twin with respect to the twin plane is a useful tool to distinguish between 100 and $\overline{1}01$ contact twins, especially for natural samples whose optical extinction angles can often be difficult to measure.

Moreover, the multiplicity of the gypsum twin operations is 2 (rotation of 180°, mirror plane or inversion center) and thus each twin law is composed of only two sub-crystals. In contrast, the experimentally obtained $\overline{1}01$ contact twins show many sub-crystals that form the twin [Fig. 3(a)]. To explain this intriguing habit, a plausible mechanism might be that when the first $\overline{1}01$ contact twin is formed – composed of only two sub-crystals – its re-entrant angle is the most reactive site, and thus a new $\overline{1}01$ contact twin can statistically nucleate and grow in this position. When this mechanism is repeated several

times, a multi-laminated twin is generated, as shown in Fig. 3. Explaining how this complex twin grows is beyond the scope of this work and will be investigated in future contributions.

3.2. The role of CO_3^{2-} ions in the formation of the $\overline{1}01$ gypsum contact twin law

Rapidcreekite is a rare hydrated Ca-sulfate–Ca-carbonate compound ($Ca_2SO_4CO_3 \cdot 4H_2O$) found in association with gypsum and other carbonate minerals (Bots, 2011; Avdontceva et al., 2021). It is composed of layers of $Ca–SO_4–Ca – CO_3$ with each Ca site coordinated by CO_3, SO_4 and two H_2O groups (Cooper & Hawthorne, 1996). It belongs to the orthorhombic *Pbcn* space group and its unit-cell parameters are $a_0 = 15.49$ Å, $b_0 = 19.18$ Å, $c_0 = 6.15$ Å, $\alpha = \beta = \gamma = 90°$ (Cooper & Hawthorne, 1996; Roberts et al., 1986; Avdontceva et al., 2021).

Due to the chemical and structural affinities between gypsum and rapidcreekite structures, Cooper & Hawthorne (1996) suggested a new formation mechanism for gypsum twins. They realized that the replacement of half the sulfate groups in gypsum produces the formula of rapidcreekite.

The resulting structure contains alternating sulfate and carbonate layers, and the sulfate groups in the alternate layers are rotated (*i.e.* twinned) by 180° with respect to the previous one (Fig. 4). Interestingly, the twin operation (*i.e.* 180° rotation) occurs along the [101] direction in our gypsum indexing,
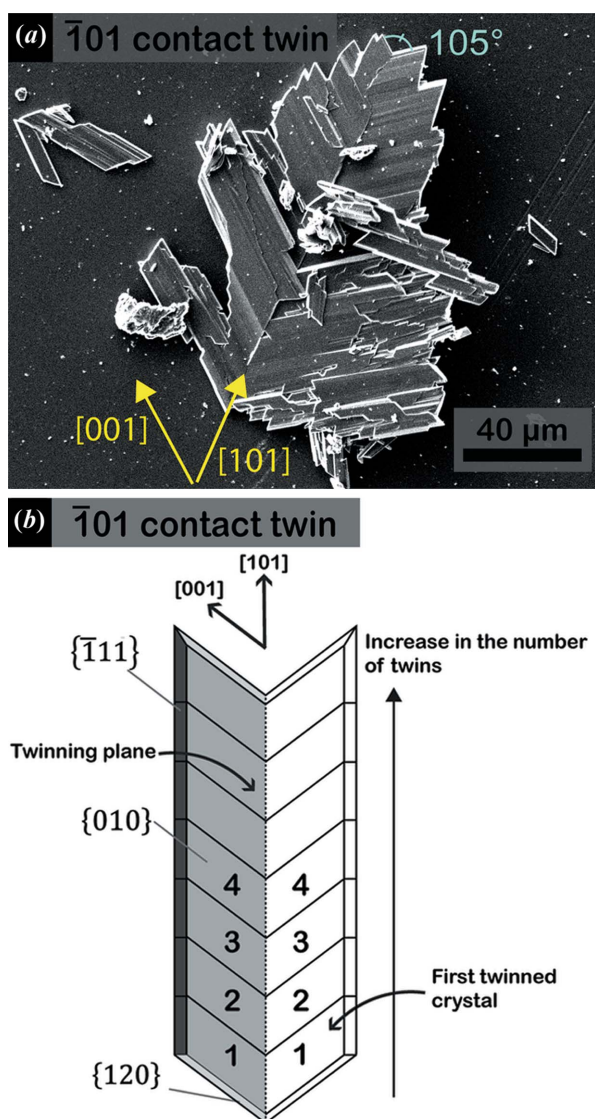

Figure 3
(a) $\overline{1}01$ gypsum contact twin precipitated from a solution saturated in Ca-carbonate and calcium sulfate dihydrate (G2 solution). (b) Schematic representation of the $\overline{1}01$ gypsum contact twins obtained in G2 solution.
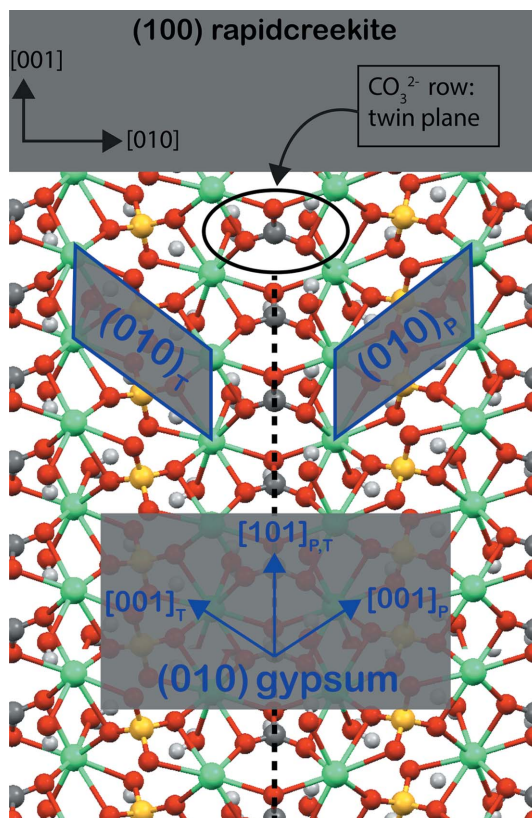

Figure 4
Projected structure of rapidcreekite perpendicular to the (100) plane: evidence that twinning in the gypsum structure can be attributed to the presence of rows of carbonate groups (black dashed line). Green – calcium; yellow –sulfur; red – oxygen; dark gray – carbon; light gray – hydrogen.

Table 1
2D lattice coincidences between the {100} form of rapidcreekite and the monoclinic {010} form of gypsum.

Rapidcreekite (100)	Gypsum (010)	Geometric misfit (%)
$[0\bar{1}2] = 22.78$ Å	$4 \times [100] = 22.52$ Å	−1.14
$[001] = 6.15$ Å	$[101] = 6.52$ Å	5.67
2D area = 118.23 Å^2	2D area = 128.59 Å^2	8.00

matching with the growth direction of the re-entrant angle in $\bar{1}01$ gypsum twins.

Moreover, the effects of carbonate species in solution on gypsum crystallization were studied by Bots (2011) through *in situ* time-resolved crystallization experiments using wide-angle synchrotron X-ray scattering (WAXS) analyses [I22 beamline (SAXS/WAXS) at Diamond Light Source]. Bots observed that rapidcreekite is an intermediate product in gypsum formation.

Such results agree with our experimental observations involving the precipitation of $\bar{1}01$ contact twins in carbonate-rich environments.

We investigated the 2D lattice coincidences between the {100} form of rapidcreekite and the {010} form of gypsum (Table 1). Both calculated linear and area misfits satisfy the constraints required for epitaxy interaction (*i.e.* linear and area misfit <14%) (Mutaftschiev, 2001), allowing us to consider rapidcreekite as a precursor in gypsum precipitation via an epitaxial mechanism, promoting the formation of the $\bar{1}01$ contact twin law. Indeed, epitaxial growth is an acknowledged phenomenon responsible for triggering different growth morphologies (Kellermeier *et al.*, 2012; Bruno *et al.*, 2022*a*) and polymorphs even if metastable phases are involved

(Bruno *et al.*, 2022*b*). The host phase forms a nanometre-thick intermediate structure whose faces act as the epitaxy substrate of the stable crystal, as reported in previous research where epitaxial relationships between two phases were investigated (Bruno *et al.*, 2022*a,b*).

3.3. Mineralogical implications

The marine and lacustrine waters from which gypsum precipitates are rich in carbonate in its different species. Therefore, it is relevant to explore whether the $\bar{1}01$ gypsum contact twins can be observed in these evaporitic environments. Gypsum crystals occur in evaporitic environments with three different contact twin habits:

(1) Prismatic habit [Fig. 5(*a*)] (Reid *et al.*, 2021) with a re-entrant angle value ranging between 100 and 105° and sub-crystals parallel to the twin plane. These features identify the 100 twin law.

(2) Tabular habit [Fig. 5(*b*)] (Natalicchio *et al.*, 2021; Costanzo *et al.*, 2019) with a re-entrant angle value ranging between 100 and 105° and sub-crystals parallel to the twin plane (Bigi *et al.*, 2022). Thus, the crystal follows the 100 twin law as shown in Fig. 5(*a*), but is characterized by a different habit.

(3) Multi-laminated habit [Fig. 5(*c*)], commonly called 'Christmas tree' (Rodríguez-Aranda *et al.*, 1995). In Fig. 5(*c*) the re-entrant angle value range is 98–101°, closer to the re-entrant angle value of 105° related to the 100 and the $\bar{1}01$ gypsum twin laws.

Five twin laws are allowed for the gypsum structure (Follner *et al.*, 2002), and consequently only five re-entrant angle values are possible. However, it is reasonable to assume that, in the natural environment, gypsum crystals may be subjected to
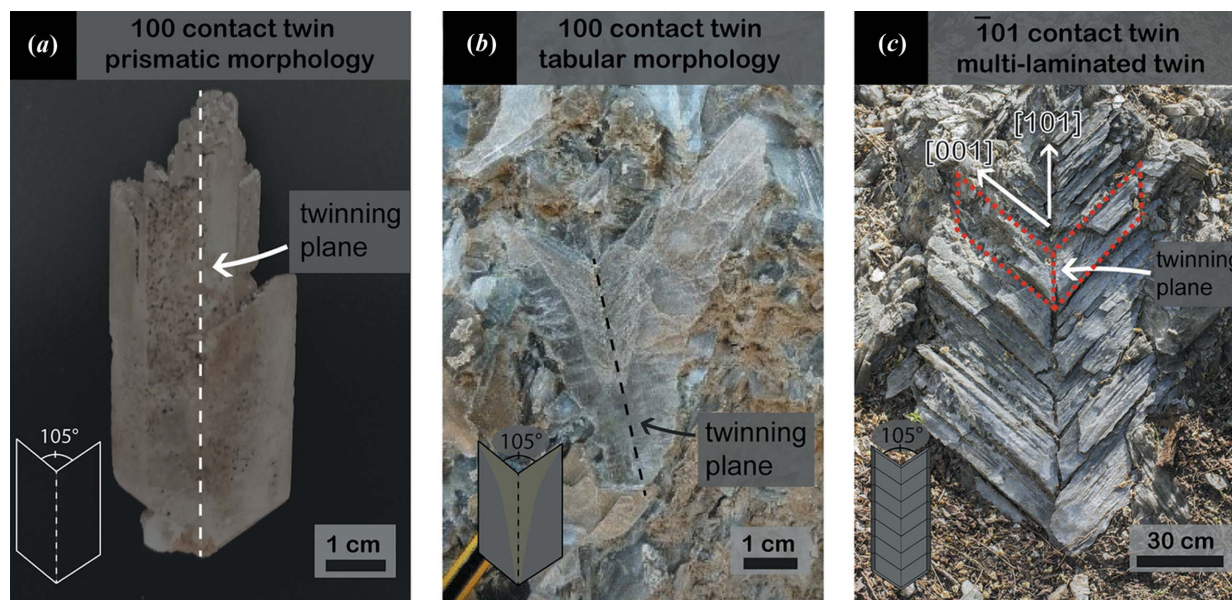

Figure 5
Examples of natural gypsum contact twins in modern and ancient evaporitic environments. (*a*) Centimetre-sized gypsum twin from the Atacama Desert, Chile. (*b*) Centimetre-sized Messinian selenitic gypsum from Piedmont basin, Italy (photograph courtesy of Marcello Natalicchio). (*c*) Metre-sized Messinian selenitic gypsum from 'Vena del Gesso Romagnola', Italy, composed of many sub-crystals obliquely elongated with respect to the twin plane (photograph courtesy of Piero Lucci).

physical processes which may result in a deviation from the theoretical value of the twin law re-entrant angle, as demonstrated by the natural gypsum twins shown in Fig. 5.

Interestingly, in Fig. 5(c) the habit is composed of many specular and bladed individuals obliquely elongated with respect to the twin plane, like the $\bar{1}01$ contact twins detected in the G2 solution. The [001] direction (c axis) is parallel to the elongation of the sub-crystals composing the twin; the same crystallographic directions describing $\bar{1}01$ contact twins detected in G2 are obtained. Therefore, we propose that the $\bar{1}01$ gypsum contact twins observed in the crystallization experiments from solutions saturated in Ca-carbonate are present in geological evaporitic environments. The high carbonate content in the brine from which the evaporites precipitate could promote the formation of this gypsum habit.

3.4. Fluid inclusion directions in $\bar{1}01$ contact twins

FIs are small droplets of fluid trapped in minerals during their growth from the fluid phase; hence, rapid crystal growth events can result in polyhedric, dendritic or irregular FIs (Roedder, 1984; Bodnar et al., 2003). However, after trapping, processes of recrystallization generally termed 'necking down' start to reduce the high surface energy of the FIs, especially in soluble minerals (Roedder, 1984; Bodnar et al., 1985; Vityk et al., 2000). The final result of such a necking down is the formation of FI morphologies reflecting those of the host mineral (Goldstein & Reynolds, 1994) at equilibrium with its mother solution, i.e. they represent the negative equilibrium shape (ES) of the host crystal.

In the 100 gypsum twins, where the two individuals that form the twin grow along the [001] direction (Otálora & García-Ruiz, 2014; Costanzo et al., 2019), the primary FIs show a negative ES elongated along the [001] direction parallel to
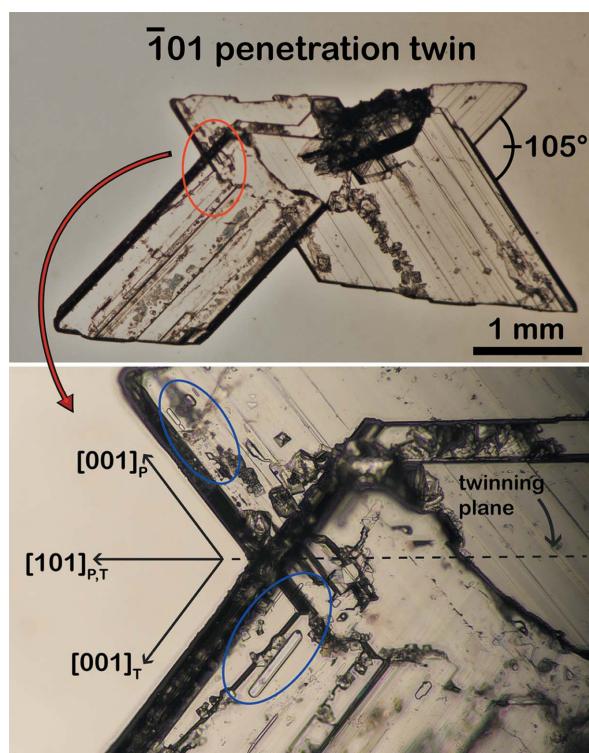

Figure 7
FIs in $\bar{1}01$ twins are elongated along [001] and oriented obliquely with respect to the twin plane.

the twin plane (Goldstein & Reynolds, 1994; Bigi et al., 2022) [Fig. 6(a)]. In contrast, in $\bar{1}01$ twins the [001] direction is oriented obliquely with respect to the twin plane, and thus, negative ES of FIs should develop obliquely with respect to the twin plane as well [Fig. 6(b)]. To test this hypothesis, optical microscopy was employed to observe FIs in millimetre-sized gypsum crystals belonging to the $\bar{1}01$ twin law (Fig. 7). The crystal shown in Fig. 7 is one of those synthesized by Krüger et al. (2013).

Fig. 7 shows FIs grown along the [001] direction, oriented obliquely with respect to the twin plane and the growth direction of the re-entrant angle. Thus, the different orientations of the primary FIs' negative ES with respect to the twin plane are a useful tool to distinguish between the 100 and $\bar{1}01$ twin laws.

4. Conclusions

In this work, the effect of Ca-carbonate on the gypsum habit was studied by carrying out temperature-controlled laboratory experiments. Starting from two aqueous solutions saturated at 40°C in $CaSO_4 \cdot 2H_2O$ (G1) and in $CaSO_4 \cdot 2H_2O$–$CaCO_3$ (G2), we obtained gypsum by decreasing the temperature from 40 to 4°C.

We observed that Ca-carbonate triggers the formation of $\bar{1}01$ gypsum contact twins. An epitaxial mechanism between the (100) face of rapidcreekite ($Ca_2SO_4CO_3 \cdot 4H_2O$) and the (010) face of gypsum ($CaSO_4 \cdot 2H_2O$) is suggested to explain the $\bar{1}01$ gypsum contact twin formation. Both the atomic and
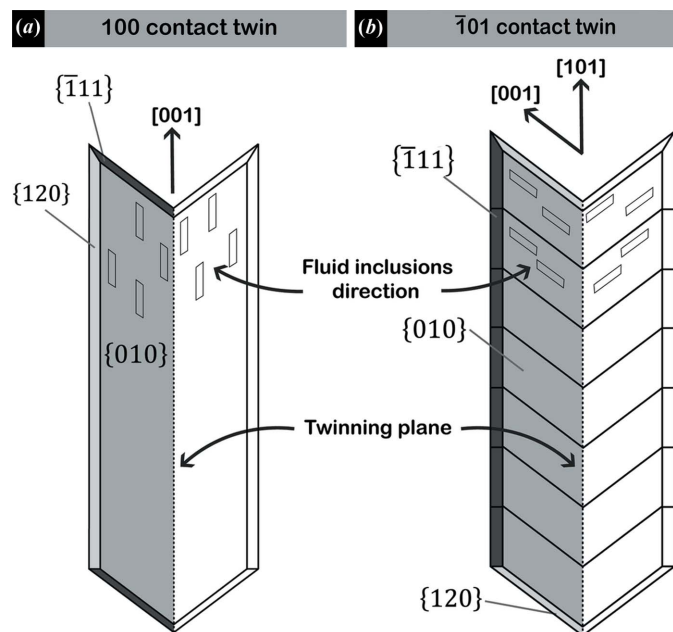

Figure 6
(a) 100 twin law, with FIs parallel to the twin plane. (b) $\bar{1}01$ twin law, where inclusions are always oriented parallel to the [001] direction of single crystals, but obliquely with respect to the twin plane.

the energetic levels of this mechanism will be discussed in detail in a forthcoming paper. Furthermore, when comparing the different gypsum twin morphologies observed in evaporitic environments with gypsum twins obtained in our experiments, we suggest that the occurrence of $\overline{1}01$ gypsum contact twins in nature is probably more common than considered, and it could be an indicator of a high carbonate concentration in the brine from which they precipitate. Finally, it has been shown that the different orientations of primary FIs' negative ES with respect to the twin plane and the main elongation of the sub-crystals that make up the twin are a useful tool to distinguish between the 100 and $\overline{1}01$ twin laws.

To summarize, our results should help others to make better use of the twin laws observed in gypsum in ancient sedimentary successions as a proxy for the chemistry of the original brine.

References

Aquilano, D., Bruno, M., Cotellucci, A., Pastero, L. & Ghignone, S. (2022). *CrystEngComm*, **24**, 5120–5127.

Aquilano, D., Otálora, F., Pastero, L. & García-Ruiz, J. M. (2016). *Prog. Cryst. Growth Charact. Mater.* **62**, 227–251.

Avdontceva, M. S., Zolotarev, A. A., Krivovichev, S. V., Krzhizhanovskaya, M. G., Bocharov, V. N., Shilovskikh, V. V., Zolotarev, A. A. & Rassomakhin, M. A. (2021). *J. Geosci.* pp. 147–156.

Bigi, D., Lugli, S., Manzi, V. & Roveri, M. (2022). *Geology*, **50**, 454–459.

Bodnar, R. J., Reynolds, T. J. & Kuehn, C. A. (1985). *Rev. Econ. Geol.* **2**, 73–97.

Bodnar, R. J., Samson, I., Anderson, A. & Marshall, D. (2003). *Fluid Inclusions: Analysis and Interpretation*, edited by I. Samson, A. Anderson & D. Marshall, Mineralogical Association of Canada Short Course Series, Vol. 32, pp. 213–230. Ottawa: Mineralogical Association of Canada.

Bots, P. (2011). PhD thesis. University of Leeds, UK.

Bruno, M., Pastero, L., Cotellucci, A. & Aquilano, D. (2022a). *CrystEngComm*, **24**, 4165–4173.

Bruno, M., Prencipe, M., Aquilano, D., Cotellucci, A., Ghignone, S. & Németh, P. (2022b). *J. Phys. Chem. C*, **126**, 6472–6481.

Canals, A., Van Driessche, A. E. S., Palero, F. & García-Ruiz, J. M. (2019). *Geology*, **47**, 1161–1165.

Cody, A. M. & Cody, R. D. (1989a). *J. Cryst. Growth*, **98**, 721–730.

Cody, A. M. & Cody, R. D. (1989b). *J. Cryst. Growth*, **98**, 731–738.

Cody, R. D. (1979). *J. Sediment. Res.* **49**, 1015–1028.

Cole, W. F. & Lancucki, C. J. (1974). *Acta Cryst.* B**30**, 921–929.

Comodi, P., Nazzareni, S., Zanazzi, P. F. & Speziale, S. (2008). *Am. Mineral.* **93**, 1530–1537.

Cooper, M. A. & Hawthorne, F. C. (1996). *Can. Mineral.* **34**, 99–106.

Costanzo, A., Cipriani, M., Feely, M., Cianflone, G. & Dominici, R. (2019). *Carbonate Evaporite*, **34**, 743–756.

Coto, B., Martos, C., Peña, J. L., Rodríguez, R. & Pastor, G. (2012). *Fluid Phase Equilib.* **324**, 1–7.

Craker, W. E. & Schiller, K. K. (1962). *Nature*, **193**, 672–673.

De Jong, W. F. & Bouman, J. (1939). *Z. Kristallogr. Cryst. Mater.* **100**, 275–276.

Edgar, L. A., Fraeman, A., Gupta, S., Fedo, C., Grotzinger, J. P., Stack, K., Bennett, K. A., Sun, V. Z., Banham, S., Stein, N., Edgett, K. S., Rubin, D. M., House, C. H. & van Beek, J. (2018). *AGU Fall Meet. Abstr.* **2018**, pp. P41A-01.

Follner, S., Wolter, A., Helming, K., Silber, C., Bartels, H. & Follner, H. (2002). *Cryst. Res. Technol.* **37**, 207–218.

García-Ruiz, J. M., Villasuso, R., Ayora, C., Canals, A. & Otálora, F. (2007). *Geol*, **35**, 327–330.

Gendrin, A., Mangold, N., Bibring, J.-P., Langevin, Y., Gondet, B., Poulet, F., Bonello, G., Quantin, C., Mustard, J., Arvidson, R. & LeMouélic, S. (2005). *Science*, **307**, 1587–1591.

Goldstein, R. H. & Reynolds, T. J. (1994). Editors. *Systematics of Fluid Inclusions in Diagenetic Minerals*. Tulsa: The Society for Sedimentary Geology.

Jafarzadeh, A. A. & Burnham, C. P. (1992). *J. Soil Sci.* **43**, 409–420.

Kellermeier, M., Cölfen, H. & García–Ruiz, J. M. (2012). *Eur. J. Inorg. Chem.* **2012**, 5123–5144.

Kern, R. & Rehn, B. (1960). *C. R. Hebd. Seances Acad. Sci.* **251**, 1300–1302.

Krüger, Y., García-Ruiz, J. M., Canals, À., Marti, D., Frenz, M. & Van Driessche, A. E. S. (2013). *Geology*, **41**, 119–122.

Langevin, Y., Poulet, F., Bibring, J.-P. & Gondet, B. (2005). *Science*, **307**, 1584–1586.

Lugli, S., Manzi, V., Roveri, M. & Schreiber, C. B. (2010). *Palaeogeogr. Palaeoclimatol. Palaeoecol.* **297**, 83–99.

Manzi, V., Lugli, S., Roveri, M. & Charlotte Schreiber, B. (2009). *Sedimentology*, **56**, 1937–1960.

Mees, F., Casteneda, C., Herrero, J. & Van Ranst, E. (2012). *J. Sediment. Res.* **82**, 37–52.

Montagnino, D., Costa, E., Massaro, F. R., Artioli, G. & Aquilano, D. (2011). *Cryst. Res. Technol.* **46**, 1010–1018.

Mutaftschiev, B. (2001). *The Atomistic Nature of Crystal Growth*. Berlin: Springer.

Natalicchio, M., Pellegrino, L., Clari, P., Pastero, L. & Dela Pierre, F. (2021). *Sediment. Geol.* **425**, 106009.

Ortí, F. (2011). *Int. Assoc. Sedimentol. Spec. Publ.* **43**, 431–464.

Otálora, F., Criado-Reyes, J., Baselga, M., Canals, A., Verdugo-Escamilla, C. & García Ruiz, J. M. (2020). *ACS Earth Space Chem.* **4**, 882–896.

Otálora, F. & García-Ruiz, J. (2014). *Chem. Soc. Rev.* **43**, 2013–2026.

Parkhurst, D.L. & Appelo, C.A.J. (2013). *Description of Input and Examples for PHREEQC Version 3G Computer Program for Speciation, Batch-Reaction, One-Dimensional Transport and Inverse Geochemical Calculations*. Denver: US Geological Survey Techniques and Methods.

Pedersen, B. F. & Semmingsen, D. (1982). *Acta Cryst.* B**38**, 1074–1077.

Plummer, L. N. & Busenberg, E. (1982). *Geochim. Cosmochim. Acta*, **46**, 1011–1040.

Reid, R. P., Oehlert, A. M., Suosaari, E. P., Demergasso, C., Chong, G., Escudero, L. V., Piggot, A. M., Lascu, I. & Palma, A. T. (2021). *Sci. Rep.* **11**, 12769.

Reiss, A. G., Ganor, J. & Gavrieli, I. (2019). *Cryst. Growth Des.* **19**, 6954–6962.

Rinaudo, C., Robert, M. C. & Lefaucheux, F. (1985). *J. Cryst. Growth*, **71**, 803–806.

Roberts, A. C., Ansell, H. G., Jonasson, I. R., Grice, J. D. & Ramik, R. A. (1986). *Can. Mineral.* **24**, 51–54.

Rodríguez-Aranda, J. P., Rouchy, J. M., Calvo, J. P., Ordóñez, S. & García del Cura, M. A. (1995). *Sediment. Geol.* **95**, 123–132.

Roedder, E. (1984). *Fluid Inclusions.* Berlin, Boston: De Gruyter.

Rubbo, M., Bruno, M., Massaro, F. R. & Aquilano, D. (2012*a*). *Cryst. Growth Des.* **12**, 264–270.

Rubbo, M., Bruno, M., Massaro, F. R. & Aquilano, D. (2012*b*). *Cryst. Growth Des.* **12**, 3018–3024.

Ruiz-Agudo, E., Álvarez-Lloret, P., Ibañez-Velasco, A. & Ortega-Huertas, M. (2016). *Cryst. Growth Des.* **16**, 4950–4959.

Shahid, S. & Abdelfattah, M. (2009). *Eur. J. Sci. Res.* **29**, 237–248.

Van Driessche, A. E. S., Stawski, T. M. & Kellermeier, M. (2019). *Chem. Geol.* **530**, 119274.

Vityk, M. O., Bodnar, R. J. & Doukhan, J. C. (2000). *Contrib. Mineral. Petrol.* **139**, 285–297.

Warren, J. K. (1982). *Sedimentology*, **29**, 609–637.

Warren, J. K. (2010). *Earth Sci. Rev.* **98**, 217–268.